POST BUCKLING ANALYSIS OF THE ARIANE 5 FRONT SKIRT (ROSETTA-MISSION)

Hermann Lehar
University of Innsbruck – Institute for Structural Analysis and Strength of Materials (IBFT), Austria

Günther Schullerer
MAN – Technologie AG, Germany

Introduction

This contribution addresses the analysis of the behaviour of the ARIANE 5 front skirt concerning the nonlinear structural stability in the launching phase of the Rosetta-Mission.

The front skirt consists of a stiffened shell structure and is part of the main stage of the ARIANE 5 (see figure 1) transmitting the booster loads into the actual launcher. The main load carrying elements are load introduction structures, circumferential frames and axial stiffened cylindrical shells.

Within the framework of the flight worthiness assessment for the Rosetta mission, a nonlinear analysis of the front skirt for two critical flight cases was performed. The contracting body for this job was MAN-Technologie AG in Augsburg, Germany.

The crucial points of the analysis strategy itself, which had to be considered for the flight worthiness assessment, were:

- Load case selection
- Boundary conditions
- Post buckling behaviour
- Imperfection sensitivity

The computations described in the following were carried out by means of the general purpose program *ABAQUS* [7], Version 6.4.1.

The employed hardware was a *SGI Origin 3800* multiprocessor machine (shared memory architecture) with 48 R14000 processors, 96 Gigabyte memory and 2.8 Terabyte high performance RAID storage installed at the IT-Centre of the University of Innsbruck.

The report focuses on the structural behaviour of the front skirt after the occurrence of local buckling phenomena as well as on the assessment of the structural sensitivity and integrity in the context of a large FE-model (1.6 million variables).

Computational Model

The overall mesh including initial and boundary conditions and the loadings were supplied by MAN-Technologie. The general set-up (see figure 1) consists of

- the lower boundary structure (LOX-Tank)
- the front skirt itself and
- the upper boundary structure composed of the vehicle equipment bay and the above structure.

Figure 2 shows in detail the FE-mesh in the front skirt region, the following table contains the problem statistics.

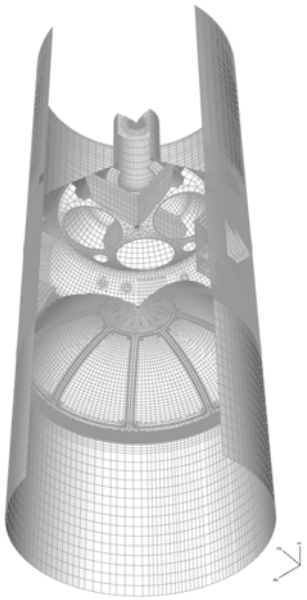

Fig. 1

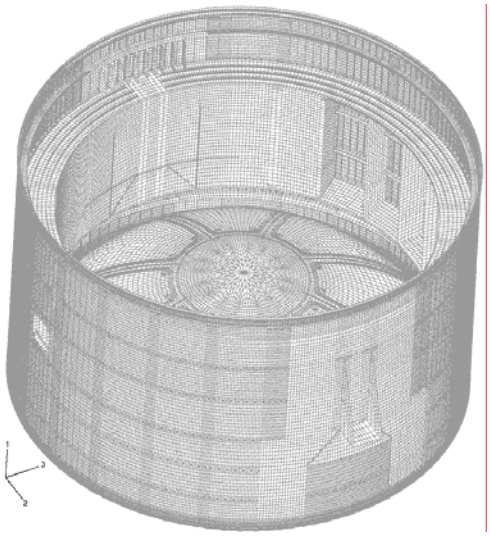

Fig. 2

Table 1

PROBLEM SIZE	
Number of elements	222756
Number of user defined elements	222684
Number of nodes	382139
Number of user defined nodes	226541
Number of generated nodes	155598
Total number of variables	1607298

This mesh basically consists of the fully integrated S4 shell element contained in the *ABAQUS* element-library [7]. The element is formulated for finite membrane strains and was chosen to avoid hourglassing.

The mesh density is based on the results of a refinement study of a linear buckling problem. The model in this refinement study was a plate, stiffened in axial direction by means of stringers. It represents a local detail of a V-Panel. The aim of the study was the investigation of the influence of different mesh sizes on the results of an eigenvalue analysis. The convergence of the mesh density was checked by controlling the relative change of the eigenvalues as the mesh was refined. The mesh should have several elements along each spatial deformation wave of the respective eigenmodes; therefore, the level of mesh refinement depends on the modes with the highest wave number in the circumferential and axial direction.

Loading

Basically four loading types have to be applied to the structure:

- the fluid pressure p_{RIE} (LOX-tank)
- the temperature field $T(t)$
- the aerodynamic pressure p_{APC} (t)
- the friction moment M_F at the booster load transmission and
- further mechanical loads L_M due to booster thrust, wind and gust.

All results presented in the following refer to a specific flight case specified by the above

mentioned loading exclusive aerodynamic pressure. The different loadings were applied in three steps with a fictitious unit step time as follows:

Step 1: Fluid pressure

Step 2: Temperature field

Step 3: Mechanical loads (M_F, L_M)

The loadings applied onto the structure are factorized according to a specific rule. Thus, the capable loading of the structure is covered by:

$$L_c = f\,(a_1\,g_{ult}\,p_{rie},\; a_2 T,\; a_3\,g_{ult}\,M_F,\; a_4\,g_{sys}\,L_M)$$

a_i being load combination factors, γ_{sys} the system margin and γ_{ult} the ultimate safety factor, respectively. Additional system margins are already included in the loads.

Initial and Boundary Conditions

The initial temperature was prescribed at all nodes to 295° K, i.e. to room temperature. Due to the panel forming process, self equilibrated residual stresses are generated in both circumferential and axial direction of the stringer-stiffened outer skin shell panels. Accounting for this effect, a uniform membrane pressure stress of 20 MPa was prescribed via initial stresses.

In order to suppress the rigid body motion of the structure, the nodes on the upper boundary were constrained to the rigid body motion of a single node, which in turn was fully constrained. This so called *multiple point constraint* (MPC) distributes the reaction forces in such a way that the resultants of the forces at the coupling nodes are statically equivalent to the force and moment at the reference node. The same technique was used to apply the loads on the lower boundary.

Constitutive Relations

The aluminium-alloy was modelled as elastic-plastic material with isotropic strain hardening. The elastic modulus, the initial yield stress and the tensile strength amount to 71600 MPa, 250 MPa and 686 MPa, respectively. The behaviour of CFP-parts was modelled as linear-elastic, orthotropic material.

Analysis Strategy

Critical points (see e.g. [1,2,3,6]), i.e. limit or bifurcation points, may occur in any sufficiently slender structure that experiences compressive stresses. Incremental-iterative methods, of which the Newton-Raphson method is the prototype, may run into difficulties at or near critical points. Essentially, those are caused by the fact that the tangent stiffness matrix $\boldsymbol{K}$ becomes singular at such points and consequently ill-conditioned in their neighbourhood. This ill conditioning can introduce 'noise' which may render the solution procedure unstable. Basically, bifurcation points are more difficult to handle than limit points and isolated critical points are easier to handle than multiple or compound critical points.

Key information when facing such a problem is the transition from stability to instability closest to the stage start. A highly accurate estimator for the singularity of the stiffness matrix $\boldsymbol{K}$ is its smallest eigenvalue. If $\boldsymbol{K}$ is real and symmetric, its eigenvalues are all real. In addition, if $\boldsymbol{K}$ varies continuously, its eigenvalues also vary continuously. Hence, a singularity is simply detected by checking for a null eigenvalue. However, an eigenvalue analysis at each increment is prohibitively expensive.

Another possible test function for the occurrence of critical points is the determinant of $\boldsymbol{K}$. If the entries of $\boldsymbol{K}$ depend continuously on a stage control parameter λ (e.g. the step time), the eigenvalues of $\boldsymbol{K}$ also depend continuously on λ. Thus the transition from strong stability to instability has to go through the neutrally stable equilibrium position, which is characterised by a null eigenvalue.

Since *ABAQUS* uses a full Newton method, a decomposition of $\boldsymbol{K}$ of the form

$$\boldsymbol{K} = \boldsymbol{L}^T \boldsymbol{D} \boldsymbol{L}$$

is performed where $\boldsymbol{L}$ is an upper triangular matrix and $\boldsymbol{D}$ is diagonal.

It is well known that the smallest entry in D, i.e. d = min(Di), also monitors the smallest eigenvalue of K. Moreover, d = 0 when K is singular and d < 0 if K is indefinite. Thus, the value of d is readily available without any overhead and plays the role of the test function adopted in ABAQUS. Once it has been determined that there is a critical point lying between two increments, one may switch to the expensive eigenvalue analysis. Occasionally it is of interest to continue the nonlinear analysis beyond critical points to investigate the post buckling behaviour. As a consequence, the problem of traversing critical points in the context of incremental-iterative methods arises.

In contrast to bifurcation points, limit points, at which the tangent to the equilibrium path is unique but normal to the λ axis, can be traversed by means of arc-length-controlled incremental methods.

These methods (e.g. the *modified RIKS-method* [10]) work well in problems where the equilibrium path in the load-displacement space is smooth and does not branch (e.g. snap-through problems).

However, if the instability is localised, there will be a local transfer of strain energy from one part of the model to neighbouring parts, and global solution methods may not work. This class of problems has to be solved either dynamically or with the aid of artificial damping, by using dashpots. In a nonlinear quasi-static analysis, viscous forces of the form

$$\boldsymbol{F} = c\boldsymbol{M}^{*}\boldsymbol{v}$$

are added to the global equilibrium equations where $\boldsymbol{M}^{*}$ is an artificial mass matrix calculated with unity density, c is a damping factor,

$$\mathbf{v} = \Delta\boldsymbol{u}/\Delta t$$

is the vector of nodal velocities and Δt is the time increment (which may or may not have a physical meaning in the context of the problem solved). While the model is stable, viscous forces and therefore the viscous energy dissipated are very small. If a load region goes unstable, the local velocities increase and consequently part of the strain energy then released is dissipated by the applied damping.

A further possible approach for traversing bifurcation points is treating bifurcation by perturbation [6]. The idea is to perturb the residual equation in such a way that the underlying regularity intrinsic to a bifurcation point is destroyed, i.e. a bifurcation point is transformed to a limit point. The problem is turned into a problem with continuous response instead of bifurcation and can therefore be solved by means of arc-length-control methods.

This is accomplished by introducing physical or geometric imperfections, so that there is some response in the buckling mode before the critical load is reached. In mathematical literature, this approach is referred to as *unfolding*.

The solution strategy used is based on introducing a geometric imperfection onto the structure.

ABAQUS offers three ways to define an imperfection:

- Buckling eigenmodes
- Displacements extracted from a previous static analysis
- Specifying the node number and imperfection values directly (if the precise shape of an imperfection is known by measurements).

If buckling eigenmodes are used to perturb the geometry, the imperfections are linear combinations of the eigenmodes determined in a pre-buckling analysis of the perfect structure (determining the most critical imperfection that leads to the lowest collapse load is still an open research issue [4]).

The response depends strongly on the imperfections, particularly if the buckling modes interact after buckling occurs. Structures with many closely spaced eigenmodes tend to be imperfection sensitive.

There are two factors that significantly alter the buckling behaviour: the shape of the imperfection and the size of the imperfection. The imperfect structure will be easier to analyse if the imperfection is large. If this is the case, the post buckling response will grow steadily before the critical load has been reached. The transition into the post buckled behaviour will be smooth and relatively easy to analyse.

Because of the above mentioned reasons, the solution strategy for solving branching problems associated with bifurcation points in the present project is straightforward:

- In a first stage a nonlinear analysis on the perfect structure is performed. To gain as close as possible the transition from stability to instability via the test function (the determinant of $\boldsymbol{K}$), the maximum time increment is chosen to a rather small value (e.g. 0.05). Restart information is written at a relatively high frequency (at every fifth increment).
- In a second stage the eigenvalues are extracted, based on the preload of the structure, just below the buckling load which is indicated by the message *negative eigenvalues*.
- In a last stage a post buckling analysis on the imperfect structure is performed, using as imperfection either linear combinations of the extracted eigenvalues or the perturbed geometry from the deflections of a previous static analysis on the perfect structure.

If a structure is imperfection sensitive, the load level achieved in the post buckling analysis is generally lower than the respective one in the first stage.

Artificial damping was only used in the first phase of the project in order to facilitate as far as possible an estimation of the load-carrying capacity of the structure.

This approach however, tends to hide the underlying problems and complicates the understanding of the behaviour of the structure while it facilitates the analysis.

Solution Control

By default, *ABAQUS* automatically adjusts the size of the time increments to efficiently solve nonlinear problems. After suggesting the first increment in each step, the sizes of the following increments are automatically adjusted based on convergence checks.

Therefore, the default values for the solution control need not be modified for most cases.

In the context of the present problem, only minor modifications of the default parameters were performed. To avoid premature cutbacks of the time increment, some default control parameters were modified, e.g. the equilibrium iteration number which is the base for checking whether the residuals are increasing in both of two consecutive iterations, from the default value 4 to 8. Additionally, the equilibrium iteration number at which the logarithmic rate of convergence check begins was changed from 8 to 10. The default tolerance used for the force and moment residual convergence was 0.005 in every analysis.

Bifurcation points may be masked out if coarse increments are taken. Hence, the allowed maximum time increment was tightened in the critical steps to ensure that the solution algorithm does not trace an incorrect path near critical points.

Perfect Structure

Aero-thermal heating of the outer skin, resulting in thermal strains, is the main trigger for instabilities in the present case. High temperature increase during the flight period starts about 60 sec after take-off. The temperature is limited to not exceed 100°C during booster flight. The cold LOX-tank and further impact from the upper stage keep the main load carrying structure (frames and ribs) at room temperature. The resulting high temperature gradient between the outer skin and the inner frames and ribs generates constraint pressure stresses in the axial as well as in the circumferential direction of the outer skin. The evolution of this effect can be

observed by means of the job information summarized in table 2. Up to a load proportionality factor *LPF = 0.5* in the second step, the structure as a whole behaves linearly. This can be seen on the linear increase of the radial displacement in the monitor node, located on the outer skin, which moves outwards. In the sixth increment, a cutback takes place and the monitor node moves back inwards.

Three increments after, the sign of the radial displacement changes, i.e. the node passes its initial position. At this step time, the first negative eigenvalue occurs, as shown by the number of negative eigenvalues n_λ in the last column of table 2.

Table 2

MONITOR NODE: 3006901 DOF: 1					
STEP	**ITER**	**LPF**	**t_{incr}**	**u_r**	**$n_\square$**
1/1	**5**	**1**	**1**	**0.000243**	**0**
2/1	5	0.1	0.1	0.000407	0
..	..	..	..	..	..
2/5	**3**	**0.5**	**0.1**	**0.00104**	**0**
2/6	3	0.525	0.025	0.00106	0
..	..	..	..	..	..
2/9	6	0.675	0.05625	–0.000239	**1**
..	..	..	..	..	..
2/12	8	0.844	0.05625	–0.00107	**4**
..	..	..	..	..	..
2/15	**4**	**1**	**0.04375**	**–0.00158**	**2**
3/1	5	0.01	0.01	–0.00152	**7**
..	..	..	..	..	..
3/16	2	0.393	0.000988	0.00072	**6**
..	..	..	..	..	..
3/20	**2**	**0.395**	**3.91E-05**	**0.000731**	**6**

Further on, the node moves inwards and additional negative eigenvalues appear and again disappear.

This is the rather typical behaviour of an imperfection insensitive structure, i.e. the structure regains stiffness immediately after traversing a critical point in a local region.

One might ask why the analysis continues although critical points have been traversed. The answer is simply that *ABAQUS* usually introduces a small artificial stiffness (a spring) to circumvent such problems as long as they are localised. This explains why *ABAQUS* attains a convergent solution until the 20th increment in the last step.

The analysis was stopped due to minimal time increments after increment 20. The achieved load proportionality factor amounts to *LPF = 0.395* which is without ambiguity too low as a *LPF = 1* refers to the serviceability load level in the last step. The following figure 3 shows the scaled deflections of the front skirt corresponding to *LPF = 0.395*.

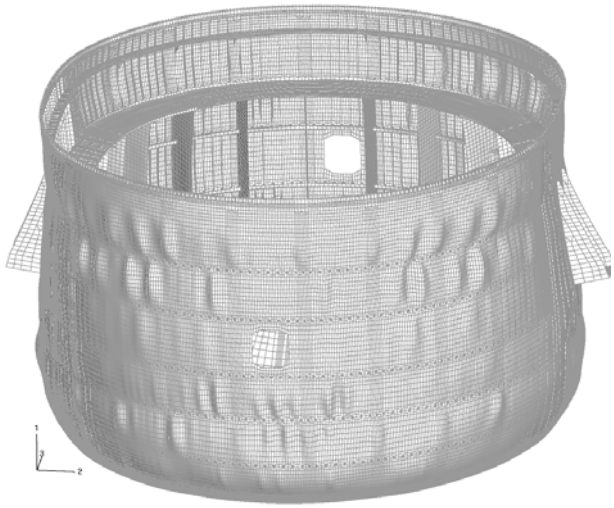

Fig. 3

Eigenvalue Analysis

The next stage in the analysis is the eigenvalue extraction, restarting the analysis from step 2 after increment 5, i.e. the last increment where restart information was written before negative eigenvalues occurred.

ABAQUS offers the so-called *Lanzcos* and the *subspace iteration* eigenvalue extraction methods. The first one is generally faster when a large number of eigenmodes is required for a system with many degrees of freedom. However, the *Lanzcos* eigensolver cannot be used for buckling analyses in which the stiffness matrix is indefinite, as for instance in models containing distributed coupling constraints (which applies in the present problem), or in a

model that has been preloaded above the bifurcation load. Hence the *subspace iteration* eigensolver was to be used. This method could also be faster when only a few eigenmodes are needed.

The reference load level matches the loading after step 1 and 50% of the loading (i.e. the temperature) applied in step 2. The live load level was set to 60% of the loading in step 2. Due to economic reasons, the number of eigenvalues to be extracted was limited to 30. The following table 3 provides the convergent positive eigenvalues. In the context of the present problem, negative eigenvalues have no physical meaning, they have therefore been omitted.

Table 3

MODE	EIGENVALUE	LPF
1	5.72421E-02	0.534345
2	5.95005E-02	0.535700
3	6.96855E-02	0.541811
4	7.01658E-02	0.542099
9	0.12346	0.574076
10	0.12427	0.574562
24	0.13846	0.583076
26	0.13885	0.583310
29	0.14175	0.585050

The *LPF* in table 3 refers to the step time of step 2 at which buckling due to thermal straining happens.

The physical time at the end of the second step being 114 seconds after the take-off, the *LPF* of the first eigenmode corresponds with a physical time of 0.534345 times 114 which yields 60.4 sec. The first eigenmode is exemplarily depicted in figure 4. Most of the remaining eigenmodes are concentrated in regions nearby the manholes.

Buckling develops in sections of the outer skin delimited by high ribs. In no case, the main load carrying structure is affected. Thus it can be preliminary concluded that the instabilities are of local nature.

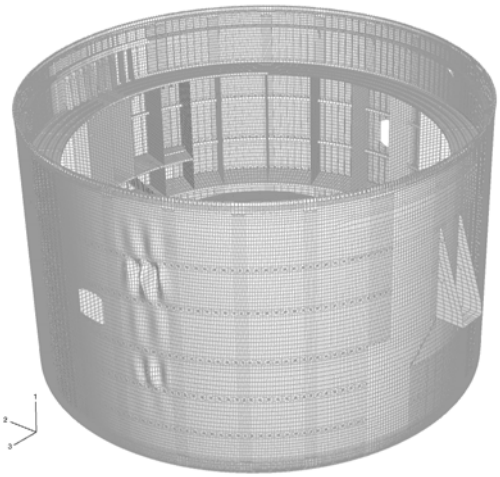

Fig. 4

Post Buckling Analysis

Following the unfolding approach, an imperfection pattern using a linear combination of the thermal eigenmodes was superimposed to the perfect geometry. Two questions arise in this context.

The first question concerns the amplitude of the imperfection, the second one the amount and the sign of the coefficients (weighting factors) for the linear combination of the eigenmodes.

Koiter [5, 8] showed that geometrical imperfections reduce the load-carrying capacity of imperfection-sensitive shells approximately in proportion to the square root of the amplitude of the imperfection.

Specifically, he established the so called *Koiter's first formula*

$$(1-\Lambda)^2 = \frac{3\sqrt{3}}{2}\frac{w_0}{h}\Lambda$$

Λ, w_0 and h being the dimensionless buckling load whose classical value equals 1, the amplitude of the initial imperfection and the shell thickness, respectively.

In the present case, the precise shape of the imperfection is known by measurements. As agreed by the contracting party the amplitude

of the imperfection referring to the manufacturing tolerances amounts to 0.4 mm.

On the other hand, the imperfect structure is always easier to analyze when the imperfection is large. Hence, the amplitude of the imperfection was increased to 3mm. This amplitude corresponds with the commonly used value of 10% of the wall thickness reported in the relevant literature, and implies additional conservatism.

Koiter's first formula results in a decrease of 8% of the critical load when using 10% as imperfection amplitude instead of the measured imperfection amplitude of 1.33% of the wall thickness.

Due to the observed minor interaction between different eigenmodes, the same weighting factor was used for all modes in the linear combination.

The chosen combination of thermal eigenmodes yields a perturbed geometry where imperfections concentrate on regions near the manholes and do not affect the overall outer skin (see figure 5).

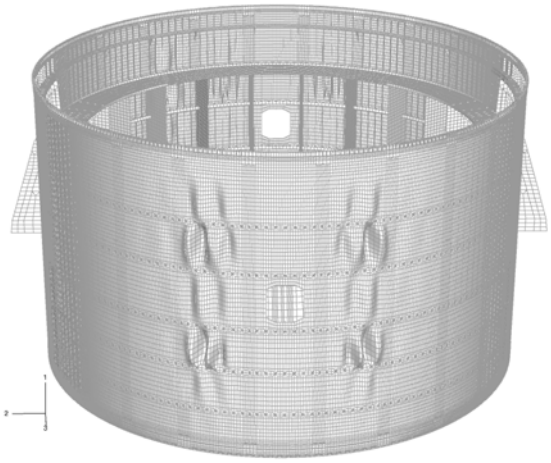

Fig. 5

The job information, summarised in the following table 4, reveals the beneficial impact of imperfections in the analysis.

Although a decreasing convergence, beginning in the 7th increment of the temperature step can be observed, the convergence in the last step is rather stable until the 36th increment, which corresponds to a *LPF = 1.94*.

Table 4

MONITOR NODE: 3006901 DOF: 1					
STEP	**ITER**	**LPF**	**t_{incr}**	**u_r**	**n_λ**
1/1	**5**	**1**	**1**	**0.000233**	**0**
2/1	5	0.1	0.1	0.000385	0
..	..	..	..	..	..
2/5	3	0.5	0.1	0.00093	0
2/6	4	0.6	0.1	0.00105	0
..	..	..	..	..	..
2/9	7	0.719	0.05625	0.00119	0
..	..	..	..	..	..
2/12	4	0.888	0.05625	0.00136	0
..	..	..	..	..	..
2/14	**5**	**1**	**0.05625**	**0.00144**	**0**
3/1	5	0.01	0.01	0.00150	0
..	..	..	..	..	..
3/16	4	1.03	0.000988	0.00717	0
..	..	..	..	..	..
3/36	**2**	**1.94**	**3.23E-04**	**0.0135**	**6**

At this steptime the convergence finally slows down. The analysis was cancelled due to the presence of negative eigenvalues indicating the final breakdown of the global structure.

Taking into account the large imperfection amplitude used in the computation, the achieved *LPF*, which corresponds to a duplication of the mechanical loads in step 3, can be judged to be adequate.

However, in order to gain a more reliable judgement of the influence of different imperfection patterns, a second analysis of the respective flight case was carried out. As a second imperfection pattern, the scaled deflections of the perfect structure in step 3 after the 20th increment (see figure 3) were superimposed to the perfect geometry.

The convergence in the last step was completely stable until *LPF = 1.75*, where it continuously slows down. The analysis was cancelled after the 57th increment corresponding to *LPF = 1.99* due to the presence of 6 negative

eigenvalues indicating the final breakdown of the global structure.

Figure 6 shows an equivalent stress contour plot of the outer skin on the deformed structure in the ultimate limit state (i.e. at *LPF = 1.99)*.

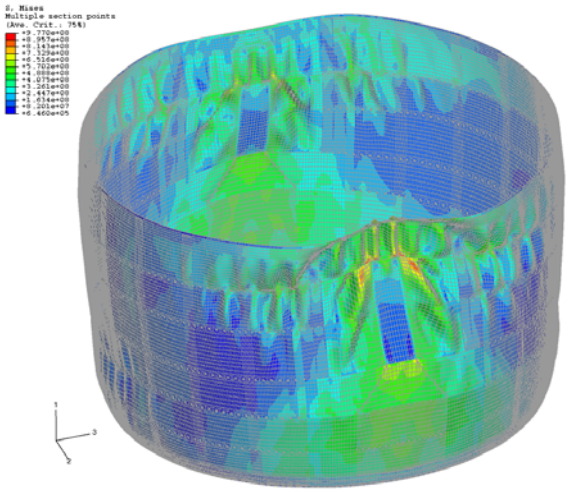

Fig. 6

The failure of the overall structure is mainly initiated by the failure of the frames.

For comparison purposes, the radial displacement vs. time diagram in the perfect case as well as in the imperfect cases (static imperfections and combined eigenmodes imperfections) of a selected node lying on the outer skin is depicted in figure 7.

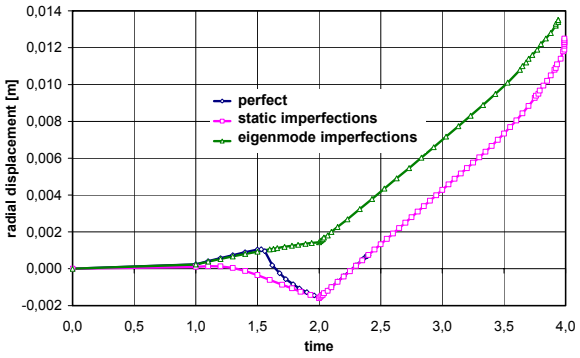

Fig. 7

Branching in a secondary path at a total time of *t = 1.5* which corresponds to the temperature field 60 sec after take-off, can be observed. Hence the node initially moves outwards and then moves inwards in the secondary path. Introducing geometric imperfections based on eigenmodes, the same node remains on the fundamental path, i.e. it moves outwards during step 2 and step 3. In contrast, when static imperfections are introduced, the node always moves continuously inwards during the temperature step and outwards in the following load step.

The respective diagrams (see figure 8) for a node lying on the outer skin in the booster load transmission area, show the same linear behaviour in all cases, irrespective of geometric imperfections.

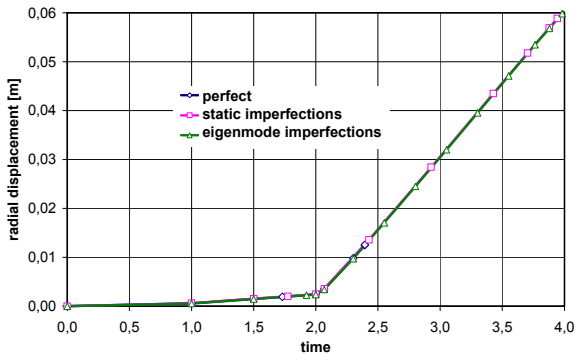

Fig. 8

Therefore, it can be concluded that the occurring instabilities during the temperature step are of local nature and hence do not diminish the load-carrying capacity of the main structure. The post critical behaviour may therefore not be expected to involve steep softening. Structures are called *imperfection-sensitive* if small imperfections have a disproportionately large effect upon their load-carrying capacity.

If different imperfections have a small effect upon the load-carrying capacity like in the present case (compare *LPF = 1.99/1.94)*, one may hypothesize that the structure is rather imperfection-insensitive.

In addition, it is known (e.g. see [6]) that imperfection-sensitive behaviour is lost when nonzero circumferential stresses are produced.

Obviously, this applies to the structure at hand because uniform heating as well as mechanical loads in the third step generate stresses both in axial and in circumferential direction.

Computational Statistics

Memory and disk estimates are summarised in table 5. The effective CPU-time for a typical eigenvalue analysis was 18.5 h, the maximum memory amounted to 16277 Mbyte. The respective values for a typical static analysis were 116.5 h and 7048 Mbyte, respectively.

Table 5

MEMORY & DISK ESTIMATES				
	RAM [Gbyte]			HD [Gbyte]
Analysis	req.	rec.	used	req.
static	1.24	5.86	7.10	3.38
eigenvalue	4.46	8.39	14.3	9.85

The total CPU-time for the analyses of two flight cases amounted to 2504 CPU-hours in a timeframe of two months.

Referring to the data given above, it can be concluded that problems of such an order of magnitude require an adequate computer.

Remarks and Conclusions

A couple of questions arose in the course of the presented analyses. They mainly pertain to the computational model, e.g. the submodel used of *ARIANE 5*, the static and kinematic boundary conditions as well as the initial conditions, the chosen loading sequence and last but not least, the analysis type referring to either static or dynamic procedure.

Although the arising processes are transient by nature, the analysed flight cases were treated as quasi-static problems with conservative loadings, which implies a load potential. The latter is a necessary condition for the solution strategy used.

Concerning the submodel technique used, it would be preferable to extract the forces applied on the boundaries of the submodel, from a coarse but comprehensive overall shell model of *ARIANE 5*.

In order to assess the influence of different loading sequences as well as initial conditions on the post critical behaviour, further studies should be conducted on small ring and stringer stiffened cylindrical shell models, representing a cut-out of the outer skin (V-Panel).

Further questions concern the reliability of the structure, i.e. the probabilistic approach [4, 8]. The latter is mandatory to gain better and more reliable information about safety and integrity. It has to be said that the resulting load factors cannot be interpreted as safety margins as those are computed in a deterministic approach. However, even in the present time, stochastic techniques would be hopelessly expensive in a nonlinear system like this. Instead of seducing the engineers into believing that risks are under total control, it is emphasized that understanding the behaviour of a structure is the central task and the key to responsible decisions in view of risks and imponderability.

Acknowledgements

The first author wishes to express his deep gratefulness for their joint effort and trust within the scope of the Rosetta project, one of the most challenging European space missions ever attempted.

Special thanks go to the staff of the IT-Centre of the Innsbruck University for their support and generous allocation of computation time and resources during this extremely time critical project.

References

[1] Arbocz J. Post buckling behaviour of structures: Numerical techniques for more complicated structures, *Lecture Notes in Physics*. Ed. H. Araki et al., Springer-Verlag, Berlin, 1987.

[2] Arbocz J. The effect of initial imperfections on shell stability, *Thin-shell structures.* Ed. Y.C. Fung, E. E. Sechler, Prentice Hall, 1974.

[3] Bazant Z. P. Stability of structures; elastic, inelastic, fracture, and damage theories. Oxford University Press, New York, Oxford, 1991.

[4] Bolotin V. V. *Statistical methods in structural mechanics*. Holden-Day, Inc., San Francisco, Cambridge, London, Amsterdam, 1969.

[5] Calladine C. R. *Theory of shell structures*. Cambridge University Press, Cambridge, New York, New Rochelle, Melbourne, Sydney, 1983.

[6] Felippa C.A. *Lecture notes in nonlinear finite element Methods*. Report No. CU-CSSC-99-xx, Center for Aerospace Structures, College of Engineering, University of Colorado, Boulder, USA, 1999.

[7] Hibbitt, Karlsson & Sorensen. *ABAQUS User's Manual, Version 6.4-1*. HKS, Inc., Pawtucket, R.I., USA, 2003.

[8] Koiter W. T. *The stability of elastic equilibrium* (in Dutch). Dissertation Thesis at the Technische Hooge School, Delft, 1945.

[9] Oberguggenberger M. The mathematics of uncertainty. *Analyzing uncertainty in civil engineering.* Ed. W. Fellin et al., Springer-Verlag, Berlin, Heidelberg, New York, 2004.

[10] Riks E. Bifurcation and stability - a numerical approach. *Innovative methods for nonlinear problems*. Ed. W.K. Liu et al., Pineridge Press, Swansea, 1984.